DTNSRDC-85/086
CALCULATION OF TWO-DIMENSIONAL NONLINEAR FLUID FLOW RESULTING FROM LARGE-AMPLITUDE FORCED HEAVE MOTION OF A U-SHAPED CYLINDER IN A FREE SURFACE

DAVID W. TAYLOR NAVAL SHIP RESEARCH AND DEVELOPMENT CENTER

Bethesda, Maryland 20084-5000

CALCULATION OF TWO-DIMENSIONAL NONLINEAR FLUID FLOW RESULTING FROM LARGE-AMPLITUDE FORCED HEAVE MOTION OF A U-SHAPED CYLINDER IN A FREE SURFACE

by

John G. Telste

APPROVED FOR PUBLIC RELEASE; DISTRIBUTION IS UNLIMITED.

COMPUTATION, MATHEMATICS AND LOGISTICS DEPARTMENT
RESEARCH AND DEVELOPMENT REPORT

December 1985

DTNSRDC-85/086

GC
1
.D3
no.85/086

MAJOR DTNSRDC ORGANIZATIONAL COMPONENTS

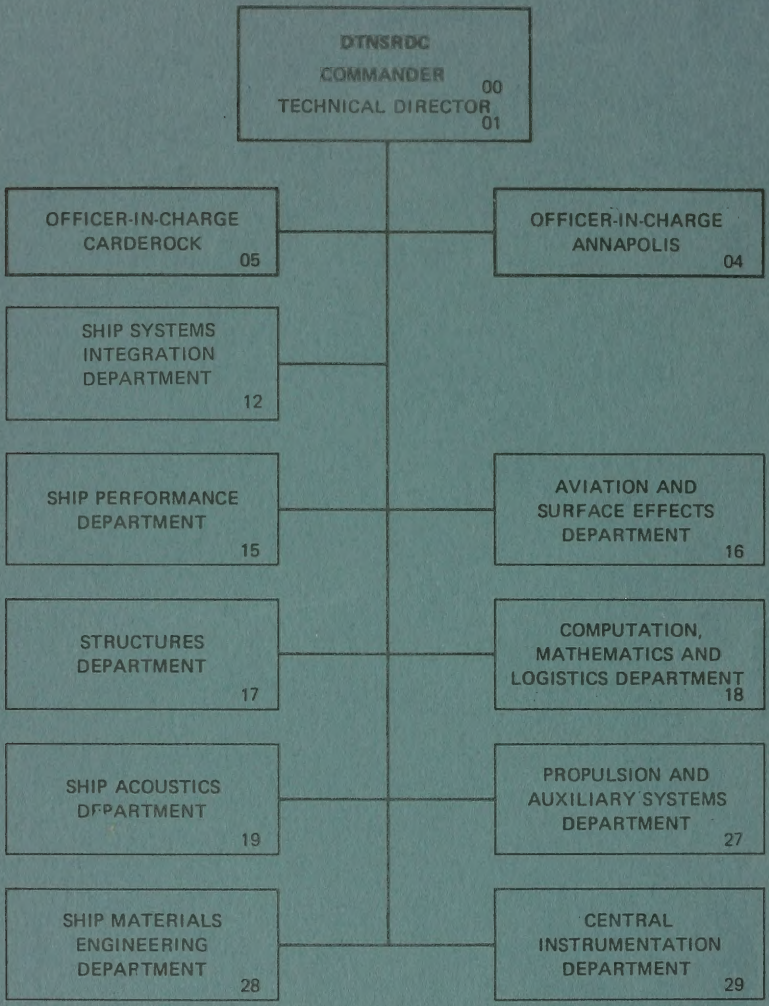

MBL/WHOI
0 0301 0039405 2

GPO 866 993

NDW-DTNSRDC 3960/43 (Rev. 2-80)

UNCLASSIFIED
SECURITY CLASSIFICATION OF THIS PAGE

REPORT DOCUMENTATION PAGE

1a. REPORT SECURITY CLASSIFICATION UNCLASSIFIED	1b. RESTRICTIVE MARKINGS
2a. SECURITY CLASSIFICATION AUTHORITY	3. DISTRIBUTION/AVAILABILITY OF REPORT APPROVED FOR PUBLIC RELEASE; DISTRIBUTION IS UNLIMITED.
2b. DECLASSIFICATION/DOWNGRADING SCHEDULE	
4. PERFORMING ORGANIZATION REPORT NUMBER(S) DTNSRDC-85/086	5. MONITORING ORGANIZATION REPORT NUMBER(S)
6a. NAME OF PERFORMING ORGANIZATION David Taylor Naval Ship Research and Development Center 6b. OFFICE SYMBOL (*If applicable*) Code 1843	7a. NAME OF MONITORING ORGANIZATION
6c. ADDRESS (*City, State, and ZIP Code*) Bethesda, MD 20084-5000	7b. ADDRESS (*City, State, and ZIP Code*)
8a. NAME OF FUNDING/SPONSORING ORGANIZATION 8b. OFFICE SYMBOL (*If applicable*)	9. PROCUREMENT INSTRUMENT IDENTIFICATION NUMBER
8c. ADDRESS (*City, State, and ZIP Code*)	10. SOURCE OF FUNDING NUMBERS PROGRAM ELEMENT NO: 61152N PROJECT NO: TASK NO: ZR0140201 WORK UNIT ACCESSION NO: DN 378003, DN 478125

11. TITLE (*Include Security Classification*)
CALCULATION OF TWO-DIMENSIONAL NONLINEAR FLUID FLOW RESULTING FROM LARGE-AMPLITUDE FORCED HEAVE MOTION OF A U-SHAPED CYLINDER IN A FREE SURFACE

12. PERSONAL AUTHOR(S)
Telste, John G.

13a. TYPE OF REPORT	13b. TIME COVERED	14. DATE OF REPORT (*Year, Month, Day*)	15. PAGE COUNT
Final	FROM _____ TO _____	1985, December	51

16. SUPPLEMENTARY NOTATION

17. COSATI CODES			18. SUBJECT TERMS (*Continue on reverse if necessary and identify by block number*)
FIELD	GROUP	SUB-GROUP	Free Surface Effects, Heaving Cylinder, Perturbation Theory, Ship Motions, Ship Hydrodynamics, Water Waves
20	04		

19. ABSTRACT (*Continue on reverse if necessary and identify by block number*)

Progress in developing a tool to compute large amplitude ship motions is reported. In particular, a method to calculate transient two-dimensional potential flow about a body moving in a free surface is described. The flow problem is formulated as an initial-boundary value problem in which the velocity potential along the free surface and the positions of the moving boundaries are sought as solutions of a coupled system of differential equations. An implicit finite-difference method is used to advance the solution of the coupled system of equations in time. The auxiliary problem of computing the velocity potential inside the fluid region is solved by a method which is based on boundary-fitted coordinates and is directly extensible to three-dimensional flows. Results from calculating the potential flow about a body in forced heave motion are presented. The hydrodynamic force on the body has been obtained and compared with the hydrodynamic force predicted from second-order perturbation theory.

20. DISTRIBUTION/AVAILABILITY OF ABSTRACT	21. ABSTRACT SECURITY CLASSIFICATION
☒ UNCLASSIFIED/UNLIMITED ☐ SAME AS RPT ☐ DTIC USERS	UNCLASSIFIED
22a. NAME OF RESPONSIBLE INDIVIDUAL John G. Telste	22b. TELEPHONE (*Include Area Code*) (202) 227-1929 22c. OFFICE SYMBOL Code 1843

DD FORM 1473, 84 MAR 83 APR edition may be used until exhausted
All other editions are obsolete

SECURITY CLASSIFICATION OF THIS PAGE
UNCLASSIFIED

TABLE OF CONTENTS

	Page
LIST OF FIGURES	iii
TABLE	iv
NOTATION	v
ABSTRACT	1
ADMINISTRATIVE INFORMATION	1
INTRODUCTION	1
MATHEMATICAL FORMULATION	4
NUMERICAL SCHEME	10
BOUNDARY FUNCTIONS	10
LAPLACE SOLVER	16
RESULTS	18
CONCLUSION	24
REFERENCES	39

LIST OF FIGURES

1 - U-Shaped Body in the Free Surface at Time t = 0.0	25
2 - Geometric Description of the Moving Body Contour	26
3 - Fluid Region for Flow Symmetric about the y-Axis	27
4 - Subregions into Which the Fluid Region is Divided	28
5 - Mesh Size in Each Subregion of the Computational Region	29
6 - Initial Mesh Near the Body	30
7 - Free-Surface Elevations Near Body for t = 5.4, 5.6, ..., 8.8	31
8 - Free-Surface Elevations Near Body for t = 9.0, 9.2, ..., 11.4	32
9 - Free-Surface Positions in a Frame of Reference Fixed to the Body for t = 6.2, 6.4, ..., 9.0	33

Page

10 - Free-Surface Positions in a Frame of Reference Fixed to the Body for t = 9.2, 9.4, ..., 12.2 34

11 - Comparison of Computed Nonlinear Force with Linear Force and with Second-Order Force as Functions of Time t 35

12 - First- and Second-Order Forces versus Frequency Number for U-Shaped Cylinder 36

13 - Phase Angle of Forces of First- and Second-Order versus Frequency Number for U-Shaped Cylinder 37

TABLE 1 - First- and Second-Order Force Coefficients 22

NOTATION

A	Constant used in describing the body contour
AB	Contour of moving body
AE	Symmetry boundary of fluid region
a	Angle parameterizing the body contour
a(e)	A function used to denote the initial relation between the parameters a and e
$a_R(t)$	Value of the parameter a at the intersection of the free surface and the body contour
BC	Free-surface boundary of fluid region
$B_x(a,t), B_y(a,t)$	Functions describing the moving body contour
b	Half-beam of the body
CD	Far vertical boundary of fluid region
ED	Bottom boundary of fluid region
e	Parameter describing free surface and wetted body contour; perturbation parameter = h_0/b
F	Dimensionless force = $F'/L^3\sigma^2\rho$
F'	Dimensional force
F_1	First-order vertical force on heaving body, normalized by $2\rho g b^2 h_0/b$
F_{20}	Second-order sinkage on heaving body, normalized by $2\rho g b^2 (h_0/b)^2$
F_{21}	Second-order vertical force on heaving body, normalized by $2\rho g b^2 (h_0/b)^2$
f	Dummy variable used to describe a convergence criterion
g	Gravitational acceleration
h	Depth of the rectangular fluid region
h_0	Amplitude of forced heave motion
j,k,ℓ	Location of a grid point

L	Length scale
M	Number of body grid points
m,n	Time levels
N	Number of free-surface grid points
$\vec{n}(a,t) = (n_x,n_y)$	Outward directed unit normal on body contour at $(B_x(a,t),B_y(a,t))$
O	Origin of Cartesian coordinate system
p	Dimensionless pressure = $p'/\rho\sigma^2L^2$
p'	Dimensional pressure
s	Arclength along the body contour
t	Dimensionless time = $t'\sigma$
t'	Dimensional time
x,y	Dimensionless Cartesian coordinates = $(x',y')/ L$
x',y'	Dimensional Cartesian coordinates
$x_B(e,t),y_B(e,t)$	Functions describing position of fluid particles along body contour
$x_F(e,t),y_F(e,t)$	Functions describing free-surface position
x_0,y_0	Coordinates of moving center of body
u,v	Velocity of a fluid particle; $u = \phi_x$, $v = \phi_y$
$v_n(a,t)$	Normal component of body-contour velocity (positive outward) at $(x_B(a,t), y_B(a,t))$
w	Half-width of the rectangular fluid region
α,β,γ	Functions of (ξ,η) describing the mapping of the fluid region onto the computational region
Δ	Laplace operator
Δt	Time increment
δ_1	Phase angle of first-order force on heaving body
δ_2	Phase angle of second-order force on heaving body

$\varepsilon_1,\varepsilon_2,\varepsilon_3$	Parameters used to test for convergence of iterative procedure
ξ,η	Coordinates in computational region
λ	Dimensional wavelength
ρ	Fluid density
σ	Frequency of heave motion
ϕ	Dimensionless velocity potential = $\phi'/\sigma L^2$
ϕ'	Dimensional velocity potential
$\phi_F(e,t)$	Dimensionless velocity potential along the free surface

ABSTRACT

Progress in developing a tool to compute large amplitude ship motions is reported. In particular, a method to calculate transient two-dimensional potential flow about a body moving in a free surface is described. The flow problem is formulated as an initial-boundary value problem in which the velocity potential along the free surface and the positions of the moving boundaries are sought as solutions of a coupled system of differential equations. An implicit finite-difference method is used to advance the solution of the coupled system of equations in time. The auxiliary problem of computing the velocity potential inside the fluid region is solved by a method which is based on boundary-fitted coordinates and is directly extensible to three-dimensional flows. Results from calculating the potential flow about a body in forced heave motion are presented. The hydrodynamic force on the body has been obtained and compared with the hydrodynamic force predicted from second-order perturbation theory.

ADMINISTRATIVE INFORMATION

This work was supported by the Numerical Ship Hydrodynamics Program at the David W. Taylor Naval Ship Research and Development Center. This Program is jointly sponsored by the Office of Naval Research under contract N0001484AF00001, NR-334-001, Work Unit 1542-019, and by DTNSRDC under its Independent Research Program, Task Area ZR0140201, Program Element 61152N, and Work Unit 1843-045.

INTRODUCTION

In recent years attention of naval architects and ocean engineers has focused on how vessels and offshore structures react to large-amplitude ocean waves. Th attention has been motivated by the capsizing of vessels in large breaking waves and structural failure due to the slamming forces associated with such waves. It is therefore of interest to have a method available to determi the forces on a floating body and how the body will react in these

extreme conditions. Since little is known of how a ship reacts even to nonbreaking waves, it would be extremely valuable to have a method available for predicting ship motions in the presence of large-amplitude nonbreaking waves. The method would be of practical value in a systematic study of how ship design changes would add stability in rough seas.

Researchers have spent much effort in devising methods for computing large-amplitude ship motions. Their work is usually based on the assumptions that the fluid is incompressible and the fluid motion is irrotational. The assumptions lead to the existence of a velocity potential, which simplifies the problem formulation. But, since the equations describing the free surface are nonlinear and cannot be linearized for large-amplitude waves, great difficulties arise in the computation of solutions to free-surface potential flow problems. When a body is present in the free surface, additional difficulties related to the intersection of the free surface and the body occur. For instance, the potential flow in the region is known to be singular. Lin et al. [1]* have recently described some aspects of the singularity. Dagan and Tulin [2] and Fernandez [3] discuss nonlinearities in fluid flow about blunt bodies. Because of the formidable difficulties, most of the work on nonlinear free surface flows has been for two-dimensional (2-D) flows.

Many authors have formulated the 2-D problem as an initial-boundary value problem whose solution is obtained from an integral equation for functions defined along the boundaries of the fluid. Longuet-Higgins and Cokelet [4] used such a method combined with a time-stepping procedure to calculate free-surface heights with no body present. Faltinsen [5] and Vinje and Brevig [6-8]

*A complete listing of references is given on pages 39 and 40.

have used the integral-equation approach in their studies of fluid motion in the presence of bodies. They make the restrictive assumption that the fluid domain is periodic and use complex-variable techniques that cannot be extended to three-dimensional problems. Greenhow et al. [9] have applied the method of Vinje and Brevig to the capsizing of a body in the free surface. Baker et al. [10] have developed a generalized vortex integral-equation technique that has been used for a body under the free surface. It is not clear whether the generalized vortex method is suitable for numerical computations when a body intersects the free surface or whether it will be computationally efficient when it is extended to three dimensions. Thus, even for computing nonlinear two-dimensional free-surface potential flows, full generality has not been attained.

This report describes progress made in developing a tool to compute large-amplitude ship motions. The method discussed is based on an initial-boundary value formulation, and it is a method that is directly extensible to three dimensions. The velocity potential along the free surface and the positions of the moving boundaries are sought as solutions of a coupled system of differential equations. An implicit finite-difference method is used to march the solution of the coupled system of equations forward in time. The auxiliary problem of computing the velocity potential inside the fluid region is solved by a finite-difference method based on boundary-fitted coordinates. Haussling [11] has presented a review of such techniques used for fluid flow problems.

Results from calculating the potential flow about a cylinder in forced heave motion are presented. The hydrodynamic force on the body has been obtained and compared with the hydrodynamic force predicted from second-order perturbation theory.

MATHEMATICAL FORMULATION

The physical flow problem is to compute transient two-dimensional flow about a body moving in a free surface. It is formulated mathematically as a potential flow problem in which the velocity potential along the free surface and the position of the moving free surface are sought as the solution to a nonlinear initial-boundary value problem.

In particular, the physical problem is to determine the fluid motion caused by the prescribed movement of a body partially submerged in a fluid and the resulting hydrodynamic force on the body. The prescribed motions are forced harmonic heave motions never so large that the body becomes completely submerged in or rises out of the fluid. The body considered in this report is a closed U-shaped cylinder. Gravity is the only body force acting on the fluid which is inviscid, incompressible, and initially at rest. The fluid motion is irrotational and thus a velocity potential ϕ' is assumed to exist. Surface tension is neglected.

All variables are nondimensionalized. Lengths are scaled by a length L characterizing the size of the body. Time is scaled by $1/\sigma$ where σ is the frequency of the body motion in radians per second. Velocities are scaled by σL; the velocity potential ϕ', by σL^2; pressure, by $\rho\sigma^2L^2$; and force, by $\rho\sigma^2L^3$. Here ρ is the fluid density. Thus, for example:

$$x' = L\,x, \qquad y' = L\,y, \qquad t' = t/\sigma\ ,$$

$$\phi' = \sigma L^2\phi\ , \quad p' = \rho\sigma^2L^2p, \quad F' = \rho\sigma^2L^3F,$$

where (x,y) are variables representing the coordinate system, t is time, p is

pressure, and F is force. The primed variables represent dimensional quantities; the nonprimed variables, nondimensional quantities.

The fluid region is described in terms of a fixed (x,y)-coordinate system chosen so that the y-axis points vertically upward and the undisturbed free surface is at y = 0 (Fig. 1). A fluid region of infinite depth and infinite lateral extent is modeled by a rectangular tank so deep that the effect of the bottom boundary is insignificant and so wide that no waves reflect from the side boundaries during the time for which the fluid motion is modeled. The rectangular tank is bounded by the lines $y = -h$, $x = w$, and $x = -w$. The contour of the body moving in the free surface is given as a function of time t and a parameter, a, by the equations

$$x = B_x(a,t) = A\,(\cos(a) - 0.1\cos(3a)) \tag{1a}$$

$$y = B_y(a,t) = A\,(\sin(a) + 0.1\sin(3a)) - h_0\cos(t) \tag{1b}$$

where A is a measure of the size of the body, a is the angle measured counterclockwise from the direction of the positive x-axis (Fig. 2), and h_0 is the amplitude of the heave motion. The position of the free surface is given in terms of a parameter e and the time t by $x = x_F(e,t)$ and $y = y_F(e,t)$. The functions $x_F(e,t)$ and $y_F(e,t)$ are to be calculated.

Since the flows considered in this paper are symmetric about the y-axis, only the half of the fluid region where $x \geq 0$ is considered (Fig. 3). The region is bounded by five curves. Across the boundaries AE ($x = 0$), CD ($x = w$), and ED ($y = -h$) there is no flow. The curved line AB, given by Equations (1a,b), is the contour of the moving body. BC is the free surface, whose location must be computed.

The velocity potential satisfies the Laplace equation

$$\Delta\phi = 0 \tag{2}$$

in the fluid region and is subject to certain boundary conditions. (Fluid velocity in the x-direction is given by $u = \phi_x$; fluid velocity in the y-direction, by $v = \phi_y$.) At a solid boundary, the normal velocity of the fluid must equal the normal velocity of the solid boundary since fluid cannot penetrate the boundary and no cavities are assumed to form in the fluid. In particular, at stationary boundaries the normal velocity must vanish. At the right vertical boundary of the flow domain, about 16 half-beams away from the body, this condition is given by

$$\phi_x = 0 \text{ at } x = w \tag{3}$$

Similarly, at the bottom boundary, about six half-beams below the free surface, vanishing normal velocity is specified by the equation

$$\phi_y = 0 \text{ at } y = -h \tag{4}$$

At the boundary AE directly beneath the body, where a symmetry condition is specified as a wall condition, the velocity potential must satisfy the equation

$$\phi_x = 0 \text{ at } x = 0 \tag{5}$$

Along the body contour, the normal velocity is known from the prescribed motion of the body. In fact, the normal velocity of the body at $(B_x(a,t), B_y(a,t))$ is

$$v_n(a,t) = n_x \partial B_x/\partial t + n_y \partial B_y/\partial t$$

where $\vec{n}(a,t) = (n_x, n_y)$ is the unit normal directed into the fluid given by

$$(n_x, n_y) = (\partial B_y/\partial a, -\partial B_x/\partial a)/[(\partial B_x/\partial a)^2 + (\partial B_y/\partial a)^2]^{1/2}$$

The required boundary condition for ϕ at $(B_x(a,t), B_y(a,t))$ on the body contour is thus

$$\frac{\partial \phi}{\partial n} = \phi_x n_x + \phi_y n_y = n_x \partial B_x/\partial t + n_y \partial B_y/\partial t \qquad (6)$$

The free-surface coordinates $x_F(e,t)$ and $y_F(e,t)$ have been parameterized in terms of e. The parameterization e is chosen such that for fixed e the functions $x_F(e,t)$ and $y_F(e,t)$ describe the path of a fluid particle. In other words, e is a Lagrangian variable. The velocity potential on the free surface is also parameterized in terms of the Lagrangian variable e by $\phi = \phi_F(e,t)$. An equation to be satisfied by $\phi_F(e,t)$ can be obtained from Bernoulli's equation, which can be expressed as

$$p + \partial\phi/\partial t + (\phi_x^2 + \phi_y^2)/2 + (g/\sigma^2 L)y = 0 \qquad (7)$$

where p is pressure, g is the acceleration of gravity, σ is the frequency of the forced harmonic heaving, and L is the characteristic length. Bernoulli's equation is valid on the free surface and throughout the fluid region. At the free surface, the pressure is assumed to be zero and a particular case of Bernoulli's equation, the dynamic free-surface boundary condition, results:

$$\frac{d\phi_F}{dt}(e,t) = \frac{D\phi}{Dt}(x_F(e,t), y_F(e,t), t) = (\phi_x^2 + \phi_y^2)/2 - (g/\sigma^2 L)\, y_F(e,t) \qquad (8)$$

Here $D/Dt = \phi_x \partial/\partial x + \phi_y \partial/\partial y + \partial/\partial t$ is the derivative following the motion of a fluid particle. The kinematic free-surface boundary condition, which

states that no fluid particle on the free surface can leave the free surface, is expressed by the two equations

$$\frac{dx_F}{dt}(e,t) = \frac{Dx}{Dt}(x_F(e,t),\ y_F(e,t),\ t) = \phi_x(x_F(e,t),\ y_F(e,t),\ t) \qquad (9)$$

$$\frac{dy_F}{dt}(e,t) = \frac{Dy}{Dt}(x_F(e,t),\ y_F(e,t),\ t) = \phi_y(x_F(e,t),\ y_F(e,t),\ t) \qquad (10)$$

At $t = 0$, the velocity potential on the free surface is given by

$$\phi_F(e,t=0) = 0 \qquad (11)$$

and the free surface is such that

$$y_F(e,t=0) = 0 \qquad (12)$$

The parameter e and the function $x_F(e,t)$ can be arranged so that

$$x_F(e,t=0) = e \qquad (13)$$

It is convenient to parameterize the fluid at the body contour by a Lagrangian variable e so that $x = x_B(e,t)$ and $y = y_B(e,t)$ along this boundary. This is possible since fluid particles along the solid boundary can never leave that boundary, except possibly to become free-surface particles at the intersection of the body and the free surface. Thus

$$\frac{dx_B}{dt}(e,t) = \frac{Dx}{Dt}(x_B(e,t),\ y_B(e,t),\ t) = \phi_x(x_B(e,t),\ y_B(e,t),\ t) \qquad (14)$$

$$\frac{dy_B}{dt}(e,t) = \frac{Dy}{Dt}(x_B(e,t),\ y_B(e,t),\ t) = \phi_y(x_B(e,t),\ y_B(e,t),\ t) \qquad (15)$$

subject to the initial conditions

$$x_B(e,0) = B_x(a(e),0) \tag{16}$$

$$y_B(e,0) = B_y(a(e),0) \tag{17}$$

where a(e) is a prescribed function.

In summary, we seek the solution of an initial-boundary value problem for $x = x_F(e,t)$, $y = y_F(e,t)$, $\phi = \phi_F(e,t)$ on the free surface and $x = x_B(e,t)$, $y = y_B(e,t)$ on the body contour, in which e is a Lagrangian variable that parameterizes the free surface and the body contour. These five functions obey the evolution Equations (8), (9), (10), (14), and (15) subject to the initial conditions (11), (12), (13), (16), and (17). The velocity potential in these equations must satisfy Equation (2) subject to the Neumann boundary conditions (3), (4), (5), and (6) and a Dirichlet boundary condition along the free surface governed by Equation (8).

The force on the body is calculated by integrating the pressure over the wetted surface of the body. Because the flow problem is symmetric about $x = 0$, the x-component of the force on the body vanishes:

$$F_x = 0 \tag{18}$$

The y-component of the force, positive upward, is given by

$$F_y = -2 \int p(a,t)\, n_y(a,t)\, (ds/da)\, da \tag{19}$$

where (n_x, n_y) is the unit normal at the body contour directed into the fluid and s, increasing in the counterclockwise direction along the body, represents arclength. Because of symmetry, the pressure is integrated over the half the

wetted length of the body given by $x = B_x(a,t)$ and $y = B_y(a,t)$ where $-\pi/2 < a < a_R(t)$. (The function $a_R(t)$ depends on the position of the intersection of the free surface and the body contour.)

NUMERICAL SCHEME

The functions $x_F(e,t)$, $y_F(e,t)$, $\phi_F(e,t)$ along the free surface and $x_B(e,t)$, $y_B(e,t)$ along the body contour obey five coupled first order differential equations in time with specified initial conditions. In addition, the velocity potential must satisfy specified boundary conditions at all times. To solve these equations a finite-difference method is used.

BOUNDARY FUNCTIONS

Each of the five boundary functions is discretized with respect to time and space using a fixed time step Δt. The discretized forms of the functions are denoted by

$$x_{Fj}^{(n)} = x_F(e_j, n\Delta t) \tag{20a}$$

$$y_{Fj}^{(n)} = y_F(e_j, n\Delta t) \tag{20b}$$

$$\phi_{Fj}^{(n)} = \phi_F(e_j, n\Delta t) \tag{20c}$$

for $j = 1, \ldots, N$, and

$$x_{Bk}^{(n)} = x_B(e_k, n\Delta t) \tag{20d}$$

$$y_{Bk}^{(n)} = y_B(e_k, n\Delta t) \tag{20e}$$

for k = 1, . . . , M. (The subscript j will be used for a free surface variable and the subscript k for a variable along the body contour.) Thus, the boundary functions are discretized into boundary grid points that are now assumed to move as if they were associated with fluid particles. The evolution Equations (8), (9), and (10) for $\phi_F(e,t)$, $x_F(e,t)$, $y_F(e,t)$ and the evolution Equations (14) and (15) for $x_B(e,t)$, $y_B(e,t)$ are applicable to these particles and are replaced by finite difference equations based on the Euler-modified method. The finite-difference equations are given by

$$x_{Fj}^{(n+1)} = x_{Fj}^{(n)} + \Delta t[\phi_{xj}^{(n)} + \phi_{xj}^{(n+1)}]/2 \tag{21a}$$

$$y_{Fj}^{(n+1)} = y_{Fj}^{(n)} + \Delta t[\phi_{yj}^{(n)} + \phi_{yj}^{(n+1)}]/2 \tag{21b}$$

$$\phi_{Fj}^{(n+1)} = \phi_{Fj}^{(n)} + \Delta t\left(\left\{\left[\phi_{xj}^{(n)}\right]2 + \left[\phi_{yj}^{(n)}\right]2 + \left[\phi_{xj}^{(n+1)}\right]2 + \left[\phi_{yj}^{(n+1)}\right]2\right\}/2 - (g/L\sigma^2)\left[y_{Fj}^{(n)} + y_{Fj}^{(n+1)}\right]\right)/2 \tag{21c}$$

$$x_{Bk}^{(n+1)} = x_{Bk}^{(n)} + \Delta t\left[\phi_{xk}^{(n)} + \phi_{xk}^{(n+1)}\right]/2 \tag{21d}$$

$$y_{Bk}^{(n+1)} = y_{Bk}^{(n)} + \Delta t\left[\phi_{yk}^{(n)} + \phi_{yk}^{(n+1)}\right]/2 \tag{21e}$$

where

$$\phi_{x\ell}^{(m)} = \phi_x(x_{G\ell}^{(m)}, y_{G\ell}^{(m)}, m\Delta t)$$

$$\phi_{y\ell}^{(m)} = \phi_y(x_{G\ell}^{(m)}, y_{G\ell}^{(m)}, m\Delta t)$$

for ℓ = j or k, m = n or n+1, and G = B or F. The initial conditions become

$$x_{Fj}^{(0)} = e_j \tag{22a}$$

$$y_{Fj}^{(0)} = 0 \tag{22b}$$

$$\phi_{Fj}^{(0)} = 0 \tag{22c}$$

$$x_{Bk}^{(0)} = x_B(a(e_k), 0) \tag{22d}$$

$$y_{Bk}^{(0)} = y_B(a(e_k), 0) \tag{22e}$$

In Equations (21a-e) and Equations (22a-e), the subscript j runs over all possible free surface grid points, and the subscript k runs over all possible body grid points. The intersection of the free surface and the body is treated as a body point obeying Equations (21d,e) subject to an initial condition given by Equations (22d,e).

The numerical scheme is implicit. An initial estimate for the five functions at the (n+1)-st time step is obtained by linearly extrapolating from two previous time steps. (For the first time step, the initial estimate is the initial condition.) The functions are corrected iteratively by using Equations (21a-e). The iterative procedure is stopped when the x- and y-values have satisfied an absolute error criterion of the form

$$|f^{(n+1,\ell)} - f^{(n+1,\ell+1)}| < \varepsilon_1 \tag{23}$$

and the ϕ-values along the free surface have satisfied the relative error criterion given by

$$|1 - \phi^{(n+1,\ell)}/\phi^{(n+1,\ell+1)}| < \varepsilon_2 \text{ whenever } |\phi^{(n+1,\ell+1)}| > \varepsilon_3$$

The superscripts $(n+1,\ell)$ and $(n+1,\ell+1)$ in Equations (23) and (24) refer to the ℓ-th and $(\ell+1)$-st corrected solutions of the system of differential equations at time step n+1. Generally, the stopping criteria for the iterative procedure in the Euler-modified method at each time step are that the maximum absolute change in the x- and y-values on the free surface and the body is $\varepsilon_1 = 0.001$ and the maximum relative change in the ϕ-values on the free surface is $\varepsilon_2 = 0.001$ for ϕ-values greater in absolute value than $\varepsilon_3 = 0.000001$.

Each of the five discrete evolution equations has ϕ_x or ϕ_y on the right side. In particular, to compute the right sides of Equations (21a-e), ϕ_x and ϕ_y along the moving boundaries of the fluid region must be computed from the solution of the Laplace equation for ϕ. The solution method for this equation is described in the next section.

To prevent numerical instabilities on the computed free surface from arising, a linear filtering scheme due to Shapiro [12] is used. The filtering scheme has been used successfully by Ohring and Telste [13], Haussling and Coleman [14], and several other researchers. It has been applied at fixed intervals of time, and has been especially helpful near the intersection of the free surface with the body contour.

Unless some method is used to maintain a reasonable grid spacing along the free surface and the body contour, grid points will congregate in some areas and become sparse in other areas. A method is used to keep a uniform distribution of points along the body contour and a prescribed distribution of grid points along the free surface. The prescribed free-surface distribution is such that the free-surface length between the body and the j-th free-surface grid point is a constant fraction of the total free-surface length

between the body and the outer boundary. The scheme allows one to follow the movement of boundary grid points within a time step as if they were fluid particles and to shift the grid points to other fluid particles at the end of each time step. To shift the grid points, cubic spline interpolation is used to fit the arclength as a function of grid point number along the free surface and the body contour. The positions of the grid points along the free surface and the hull are shifted and the values of all pertinent functions interpolated, using the cubic splines, to their new values. The redistribution of grid points, of course, affects the initial guess for the Euler-modified method at time step n+1. However, if the shifting is done every time step and the time step is sufficiently small, the redistribution scheme has been found to proceed smoothly.

Because of numerical errors, grid points cannot be expected to remain exactly on the body as the solution of the initial-boundary value problem is advanced in time. Numerical errors arise from the redistribution scheme and from replacing the differential equations by finite difference equations. To correct for such errors, grid points that move off the body are shifted back to the body. This is accomplished by computing the counterclockwise angle about the center of the body from the direction of the positive x-axis (Fig. 2). Every body grid point at a location slightly off the body surface at a certain value of that angle is relocated to the point on the body having the same value of that angle.

At the intersection of the free surface and the body contour difficulties arise. At this point both the free-surface boundary conditions and the boundary conditions associated with the solid boundary apply at a particular instant of time. However, the fluid particle at the intersection may move to

a position on the free surface or may move to a position on the body below the surface. In other words, the intersection point may not move with the fluid. Since the free-surface and hull boundary conditions all involve time derivatives following the fluid motion, they cannot, in general, be directly applied over a time interval to predict quantities at the intersection point. Special methods for handling this point must be developed. However, for heaving motions of an almost wall-sided body, the intersection will be essentially a fluid particle. Therefore for the current study, the body Equations (14) and (15) are applied directly at this point. Inaccuracies in this approach will become apparent in the form of a deviation from zero of the pressure at the intersection point. In fact, such pressure deviations might be used in a method to more accurately follow the intersection point as would be necessary for more complicated body shapes. One such scheme has been tested but has proved to be numerically unstable.

The pressure at all the grid points along the body including the intersection is calculated from a finite-difference version of Bernoulli's equation:

$$p_k^{(n+1/2)} = \left(\left[\phi_{xk}^{(n)} \right]^2 + \left[\phi_{yk}^{(n)} \right]^2 + \left[\phi_{xk}^{(n+1)} \right]^2 + \left[\phi_{yk}^{(n+1)} \right]^2 \right) / 4 - (g/\sigma^2 L) \left[y_k^{(n+1)} + y_k^{(n)} \right] / 2 \qquad (25)$$

The pressure is the pressure at the k-th fluid particle on the body at time $t = (n+1/2)\,\Delta t$. The force on the body at this time is calculated by numerically integrating the pressure along the body contour. Trapezoidal quadrature is used.

LAPLACE SOLVER

To solve the Laplace equation for ϕ, a finite difference method based on boundary fitted coordinates, due to Thompson et al. [15], is chosen. The finite-difference method involves mapping the time-dependent fluid region onto a fixed computational region. The coordinates ξ and η in the computational region are such that they obey the Laplace equation with x and y as dependent variables:

$$\xi_{xx} + \xi_{yy} = 0 \tag{26a}$$

$$\eta_{xx} + \eta_{yy} = 0 \tag{26b}$$

The boundary conditions for ξ and η along a given boundary are Dirichlet if a particular mesh distribution along the boundary is prescribed. The boundary condition of one coordinate is Dirichlet and that of the other coordinate is Neumann if mesh orthogonality near a particular boundary is desired.

Since all computations are to be done in the fixed (ξ,η)-computational region, it is convenient to interchange the independent and dependent variables. When this is done, the Equations (26a,b) for ξ and η become

$$\alpha x_{\xi\xi} - 2\beta x_{\xi\eta} + \gamma x_{\eta\eta} = 0 \tag{27a}$$

$$\alpha y_{\xi\xi} - 2\beta y_{\xi\eta} + \gamma y_{\eta\eta} = 0 \tag{27b}$$

where

$$\alpha = x_{\eta}^2 + y_{\eta}^2 \tag{27c}$$

$$\beta = x_{\xi} x_{\eta} + y_{\xi} y_{\eta} \tag{27d}$$

$$\gamma = x_{\xi}^2 + y_{\xi}^2 \tag{27e}$$

To obtain a mesh that wraps around the body and conforms to the other boundaries, the physical fluid region is divided into several subregions (Fig. 4). Each subregion is mapped onto a rectangle of computational space. In each rectangle of computational space, the inverted Laplace equation is solved subject to Dirichlet boundary conditions, transformed Neumann boundary conditions, or matching boundary conditions where rectangles overlap.

The Laplace equation for the velocity potential ϕ transforms exactly as Equations (26a,b). The transformed Laplace equation is given by

$$\alpha\phi_{\xi\xi} - 2\beta\phi_{\xi\eta} + \gamma\phi_{\eta\eta} = 0 \qquad (27f)$$

where α, β, γ, are defined by Equations (27c-e).

Wherever possible, central differencing is used to discretize Equations (27a-f). At the boundaries of the fluid region where a Neumann boundary condition is specified, second-order one-sided finite differences replace some of the derivatives in Equations (27a-f). (See Coleman and Haussling [16] for more details.) The resulting system of quasilinear equations for x, y, and ϕ at the grid points is solved by successive overrelaxation.

Lin et al. [1] cite the works of various researchers who show that a logarithmic singularity exists in the velocity potential of free-surface potential flow near the intersection of the free surface with a vertical wavemaker in horizontal motion. But, since the body contour for the problem considered is nearly vertical at the intersection with the free surface and since the horizontal velocity component of the body is zero, the logarithmic singularity in the velocity potential may be relatively weak. Thus special numerical treatment of the singularity may not be critical. In fact, nothing special has been included in the numerical method to accommodate such a singularity if it should arise.

RESULTS

Several forced harmonic heave motions of the U-shaped body in the free surface have been considered. The shape of the body has been fixed by setting the parameter A in Equations (1a,b) to 0.7407 in all cases. With A set to this value, the half-beam of the body and the draft of the body are both 0.6667. Amplitudes considered were $h_0/b = 0.05$, 0.3, and 0.4, in which h_0 is the amplitude of the motion and b is the half-beam of the body. Most researchers consider values of the frequency parameter $b\sigma^2/g$ that lie between 0.0 and 2.0. In this study the frequency parameter is restricted to lie in the interval from 1.5 to 2.0 since this interval contains the frequencies for which nonlinear effects are greater.

Linear theory for the problem of an oscillating body in a fluid of infinite depth and lateral extent predicts that the wavelength far from the body will approach

$$\lambda/L = 2\pi g/L\sigma^2 = 2\pi(b/L)g/b\sigma^2$$

asymptotically in time [17]. The dimensions of the rectangular tank are taken to be about one such wavelength deep and four wavelengths in half-length. Thus, if the frequency parameter $b\sigma^2/g$ is no smaller than 1, the depth h should be about 4 and the length should be about 16. This region is long enough that no waves will reach the side boundary during the first few periods of forced motion. Since the region is more than half a wavelength deep, the effects of finite depth can be ignored.

The fluid region has been divided into five time-dependent subregions. Each subregion has been mapped onto a fixed rectangle of computational space (Figs. 4, 5). The size of the mesh in each of these subregions has been depicted in Figure 5. A total of 2916 grid points, counting twice those

points where two subregions overlap, has been used for the grids that cover the computational and fluid regions. There are 34 equally spaced grid points on the half-body contour. At the far right vertical boundary, at the bottom horizontal boundary, and at the vertical boundary below the body, grid points position themselves in a way that makes the mesh near these boundaries orthogonal. At the far right boundary there are 25 grid points; at the bottom boundary, 102 grid points; on the vertical boundary directly beneath the body, where a symmetry condition is specified as a wall condition, 18 points. The initial distribution of grid points on the free surface is arranged so that the mesh near the intersection of the free surface and the body is approximately uniform in both the x- and y-directions (Fig. 6), and the mesh near the intersection of the free surface and the far right boundary is also approximately uniform in both directions. There are 90 grid points along the free surface.

The iteration for the solution to the Laplace equations for the changing mesh and for the velocity potential is done simultaneously. It is found that the mesh does not change greatly from time step to time step and hence a test for the convergence of ϕ suffices. This convergence test is that the square root of the sum of the squares of the residuals at the 34 body points should be less than 0.001. A spot check of the solution iterates indicated that the relative change in ϕ near the body was about 0.1 percent when the criterion was satisfied.

For the solution of the Laplace equations, an overrelaxation factor of 1.4 was chosen for grid points inside the computational region. For grid points on the body, where a Neumann boundary condition is specified, such a large relaxation factor caused instabilities in the solution process for ϕ.

The instabilities first appeared in areas where the body curvature was large. No completely satisfactory explanation of the problem was found, but numerical experimentation led to the use of underrelaxation factors between 0.75 and 1.0 on the body. Such underrelaxation factors on the body eliminated the instabilities.

Figures 7-10 depict some results of computing the free-surface position during the first two periods of forced motion with the amplitude such that $h_0/b = 0.4$ and the frequency such that $b\sigma^2/g = 2$. A time step of $\Delta t = 0.02$ resolved one period of motion into about 314 time steps. Figures 7 and 8 show the free surface and the body with a fixed coordinate system. Figure 7, corresponding to times between 5.4 and 8.8, shows a rising body and a sinking free surface near the body; Figure 8, for times between 9.0 and 11.4, shows a descending body and a rising free surface. Figures 9 and 10 show similar results, but the coordinate system in these figures is fixed to the heaving body. The time-dependent details of the free surface near the body are clearer in this frame of reference. Figure 9 shows a rising body between the times 6.2 and 9.0; Figure 10, a descending body between the times 9.2 and 12.2. It is interesting to note that the slope of the free surface near the body is largest at about the time the body has attained its maximum height. Results for computing the vertical force on the heaving U-shaped body are depicted in Figure 11. From the figure it is seen that the force has become periodic in less than one period of forced motion. Also shown on the figure is a curve of the force versus time predicted from the second-order theory of Papanikolaou and Nowacki [18]. The other curve is a linear magnification of the results from calculating the force when the amplitude of motion is eight times smaller ($h_0/b = 0.05$) but the frequency of the motion is the same.

Qualitative agreement among the curves appears to be good. The deviation between the computed nonlinear force and either the linear or the second-order force represents aspects of force which could not be predicted from linear or second-order theory.

Another comparison of the computed force with the force predicted by second-order theory is obtained from a Fourier analysis of the curve of force versus time for the last period of forced motion. According to second-order theory, the total dimensional force on the body when its center (x_0,y_0) oscillates vertically according to the formula $y = h_0 \sin(\sigma t)$ is given by

$$F = 2\rho g A\ (0.97\pi/4) + 2\rho g b^2 e F_1 \sin(\sigma t + \delta_1) + 2\rho g b^2 e^2 F_{20} + 2\rho g b^2 e^2 F_{21} \sin(2\sigma t + \delta_2) \qquad (28)$$

where $e = h_0/b$ is the perturbation parameter. The first term represents the hydrostatic force on the body at its neutral water position. The second term represents the first-order force on the body, and the last two terms represent second-order modifications to the first-order force on the body. A Fourier analysis of the computed nonlinear force versus time curve will produce coefficients of the Fourier expansion in the orthogonal functions $\{1, \sin(nt), \cos(nt)\}$. The coefficients are obtained from the usual integrals by numerical integration. In the case of the computed nonlinear force, the center of the body (x_0,y_0) oscillates vertically according to the formula $y_0 = h_0 \cos(\sigma t)$ instead of $y = h_0 \sin(\sigma t)$. After considering this difference, the nonlinear results can be used to arrive at the five parameters describing the force in Equation (28). The procedure, of course, assumes that the contribution to the force from third-order effects is insignificant. Table 1 shows how the computed results compare with those of Lee [17], and

Papanikolaou and Nowacki [18]. The computed results seem to be good except for the second-order amplitude F_{21}. The discrepancy in the second-order force amplitude is probably due to insufficient accuracy in the computed nonlinear force. Since first-order contributions to the force are dominant, the

TABLE 1 - FIRST- AND SECOND-ORDER FORCE COEFFICIENTS

	Lee	Papanikolaou and Nowacki	Computed Nonlinear Results
F_1	0.69	0.68	0.67
δ_1	350°	357°	357°
F_{20}	-0.2	-0.19	-0.23
F_{21}	0.62	0.68	0.82
δ_2	5°	107°	108°

relative accuracy of the remaining force when the first-order predictions are subtracted is small. The error is compounded since values calculated from the remainder are divided by the square of the perturbation parameter, a small number, to get F_{20} and F_{21}. The computed second-order phase angle is, however, excellent.

A rough estimate of the accuracy of the force computations can be obtained from two sets of computations in which only the time step is different. One such numerical test was conducted for this problem with the frequency parameter $\sigma^2 b/g = 1.7$ and the amplitude of the motion such that $h_0/b = 0.3$. The two time steps used were $\Delta t = 0.02$ and $\Delta t = 0.01$. After about $t = 2$, the average difference in the computed force was less than one percent. Thus the error seems to be quite small.

Various frequencies of forced motion have been considered for the amplitude corresponding to $h_0/b = 0.3$. Predictions of the coefficients for second-order theory were made and compared with those of Papanikolaou and Nowacki [18], Potash [19], and Lee [17]. The results are presented in Figures 12 and 13. The computed first-order coefficients agree well with the previously computed results. The computed second-order phase angle agrees well with the results of Papanikolaou and Nowacki. The magnitude of the sinkage (the third term in Equation (28)) agrees well with the previously computed results, but the magnitude of the oscillatory part of the second-order force does not agree so well. This is a reflection of the relative error in the nonlinear force when the first-order force, accounting for most of the force, has been subtracted. It is doubtful that there is more than about one digit of accuracy in the computed second-order results. To obtain these results, the fluid motion resulting from about two periods of forced harmonic oscillation was computed, and the force for the last period of the motion was decomposed into its Fourier components.

CONCLUSION

A computer program to compute the fluid motion resulting from forced harmonic heaving of a U-shaped body in a free surface has been produced. The program computes forces in reasonable agreement with the results of previous researchers who used second-order perturbation theory. The forces have been computed for cases of significant nonlinear fluid motion.

The computer program will be modified to handle a variety of body shapes and motions. Unlike the complex-variable techniques of Faltinsen [5] and Vinje and Brevig [6-8], the method chosen to solve the problem is extensible to the problem of 3-D nonlinear ship motions. The fluid domain has not been assumed periodic, as was assumed by Vinje and Brevig [6-8]. The location of the intersection of the free surface and the body has not been found from extrapolation, as was used by Vinje and Brevig [7].

Additional research needs to be performed before this method can be applied to the general problem of ship motions in two or three dimensions. Satisfactory results have been obtained for a heaving U-shaped cylinder, but heaving wedge-shaped bodies or blunt bodies in horizontal motion in the free surface are known to have more singular fluid flow behavior. Before such behavior can be treated properly, a more sophisticated treatment of the flow near the hull/water surface intersection will be required. Such a treatment should include both the dynamic free-surface equation and the kinematic condition associated with the solid boundary of the cylinder.

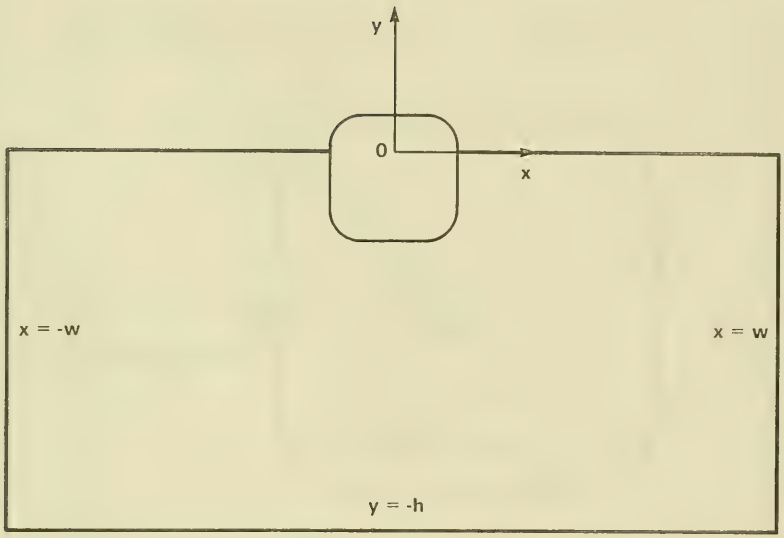

Figure 1 - U-Shaped Body in the Free Surface at Time t = 0.0

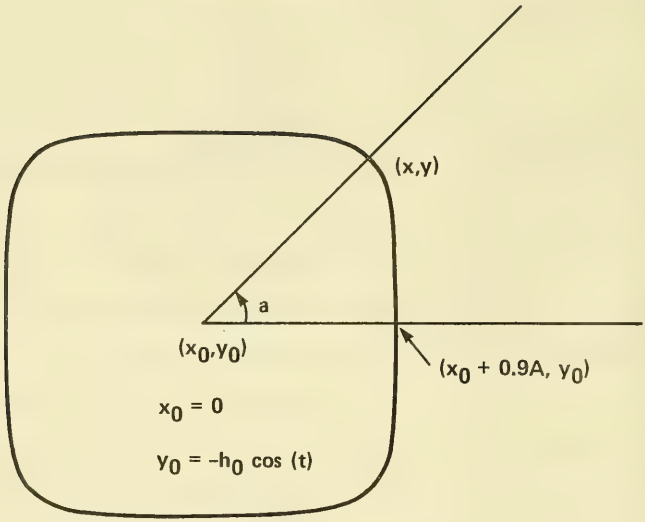

$$x = x_0 + A(\cos(a) - 0.1 \cos(3a))$$
$$y = y_0 + A(\sin(a) + 0.1 \sin(3a))$$

Figure 2 - Geometric Description of the Moving Body Contour

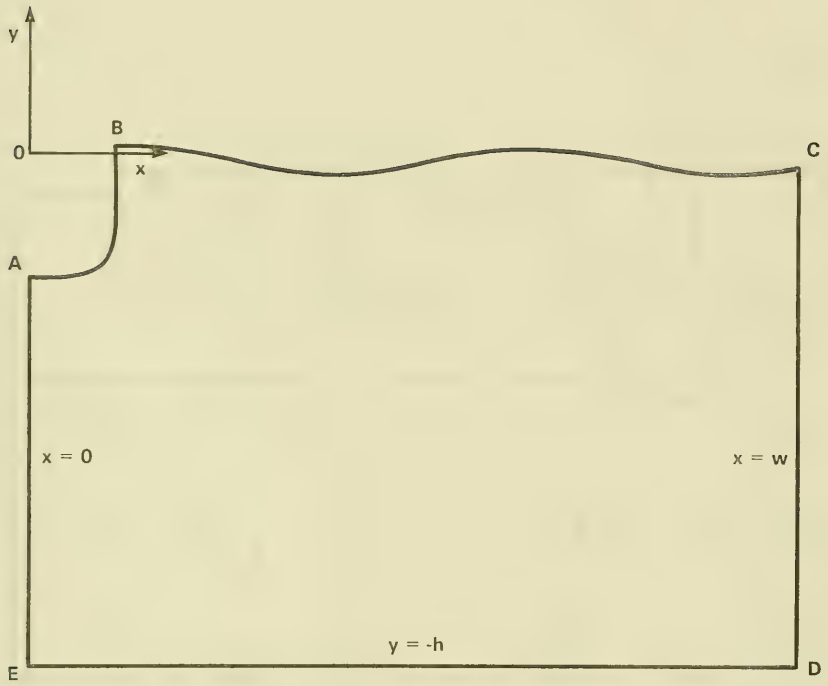

Figure 3 - Fluid Region for Flow Symmetric about the y-Axis

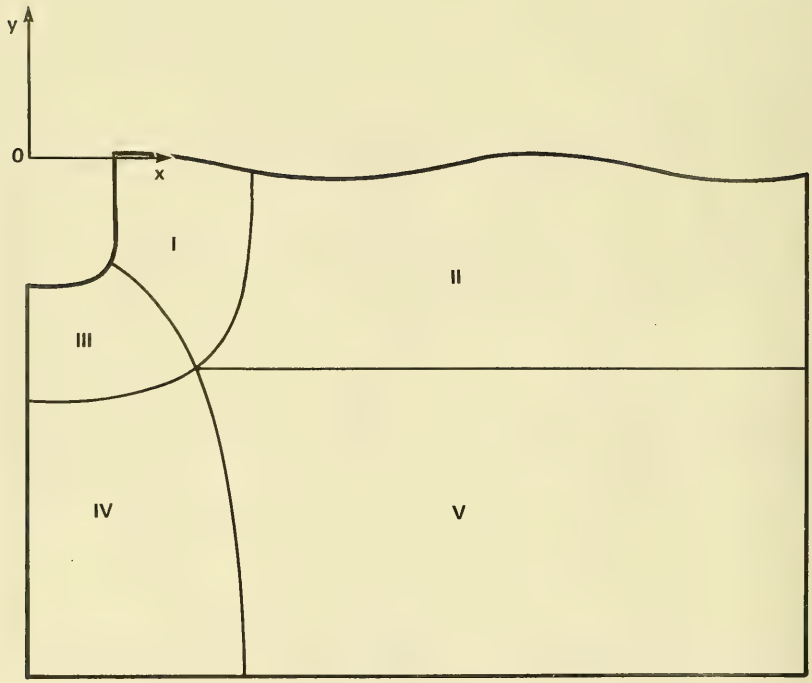

Figure 4 - Subregions into Which the Fluid Region is Divided

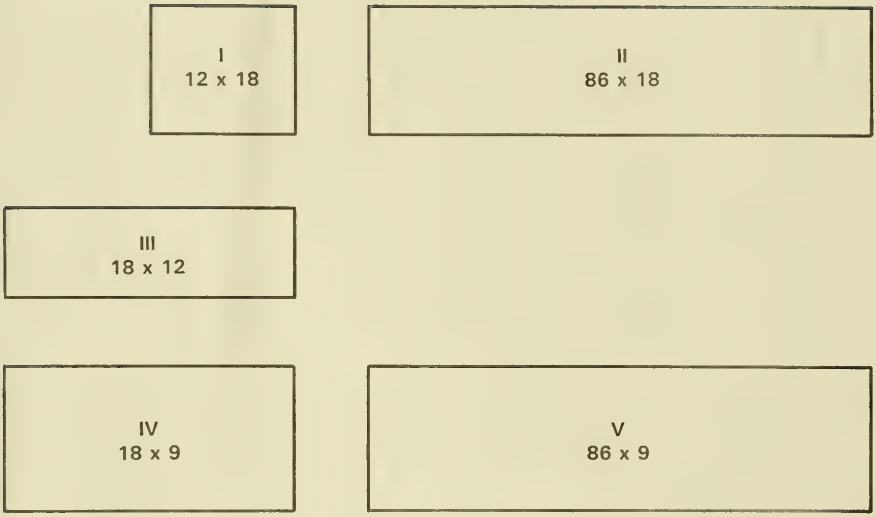

Figure 5 - Mesh Size in Each Subregion of the Computational Region

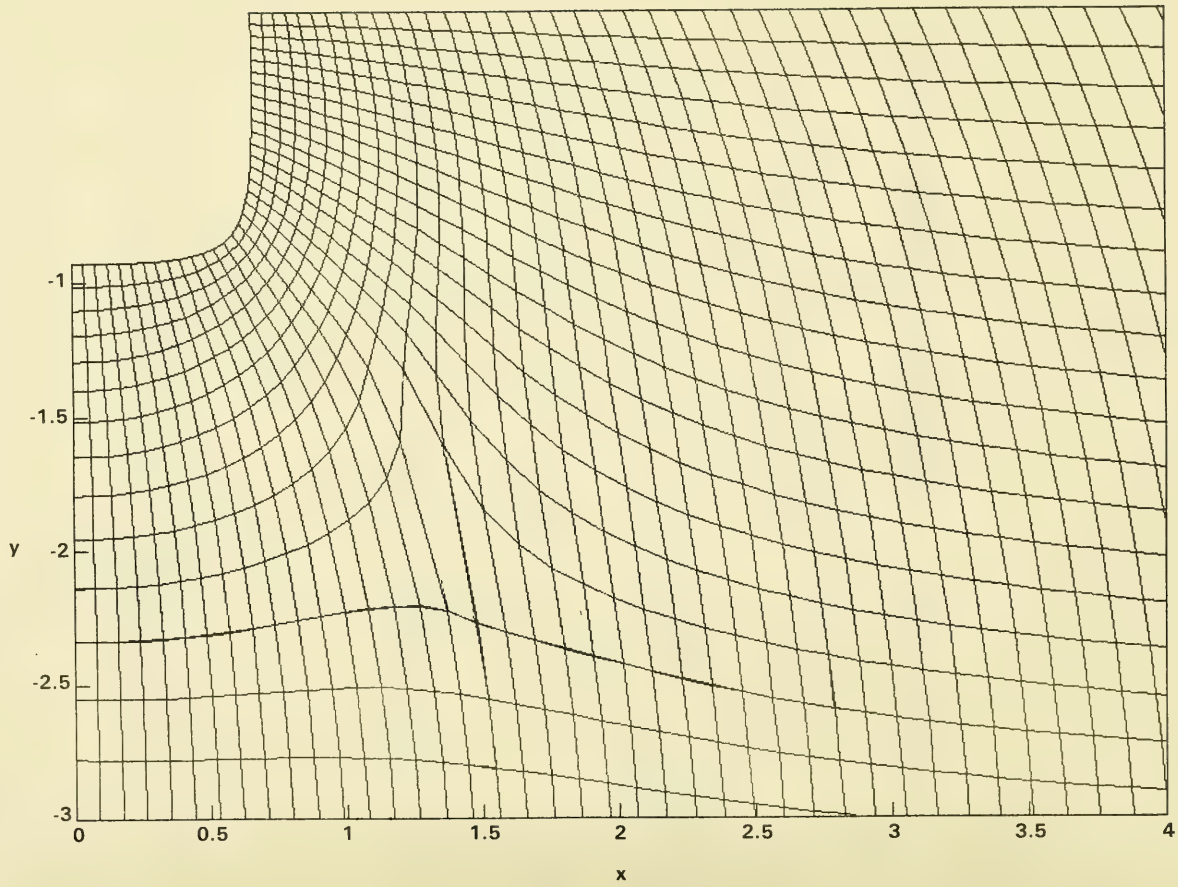

Figure 6 - Intital Mesh Near the Body

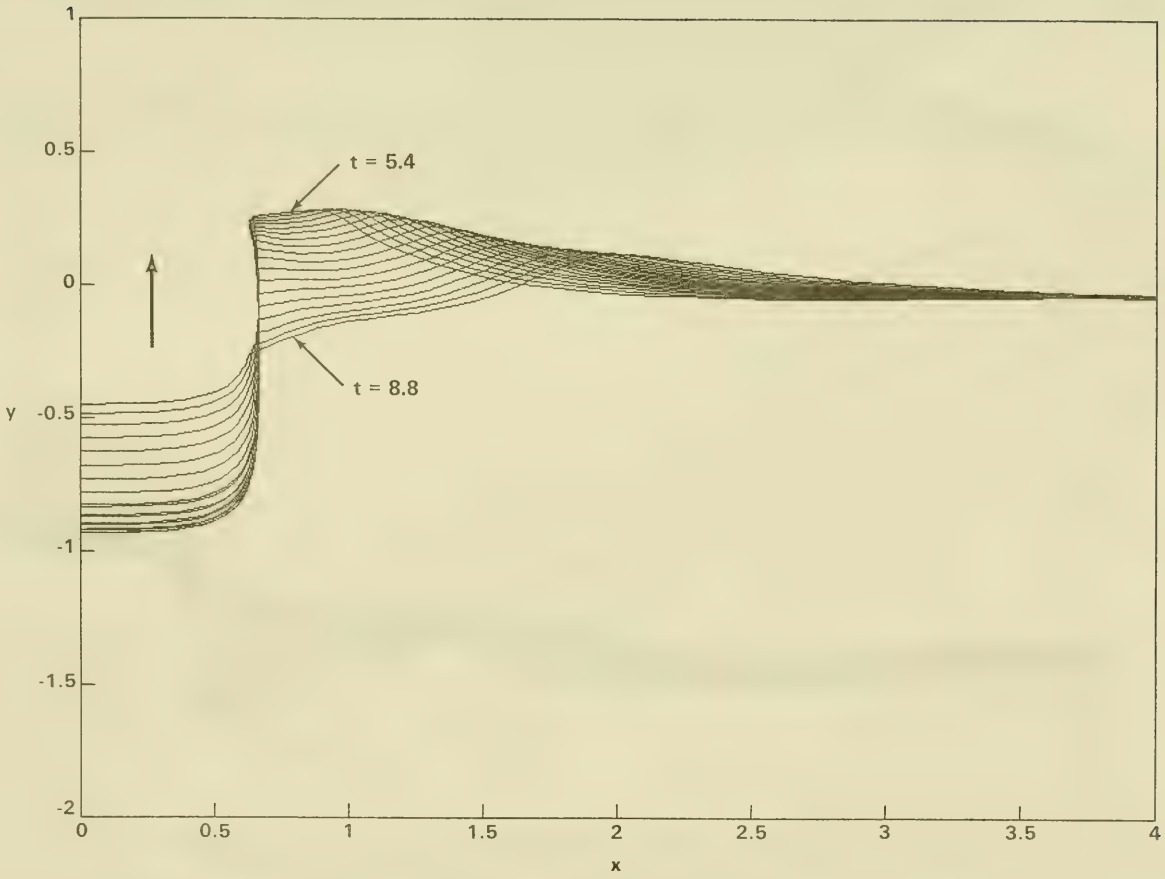

Figure 7 - Free-Surface Elevations Near Body for t = 5.4, 5.6, ..., 8.8

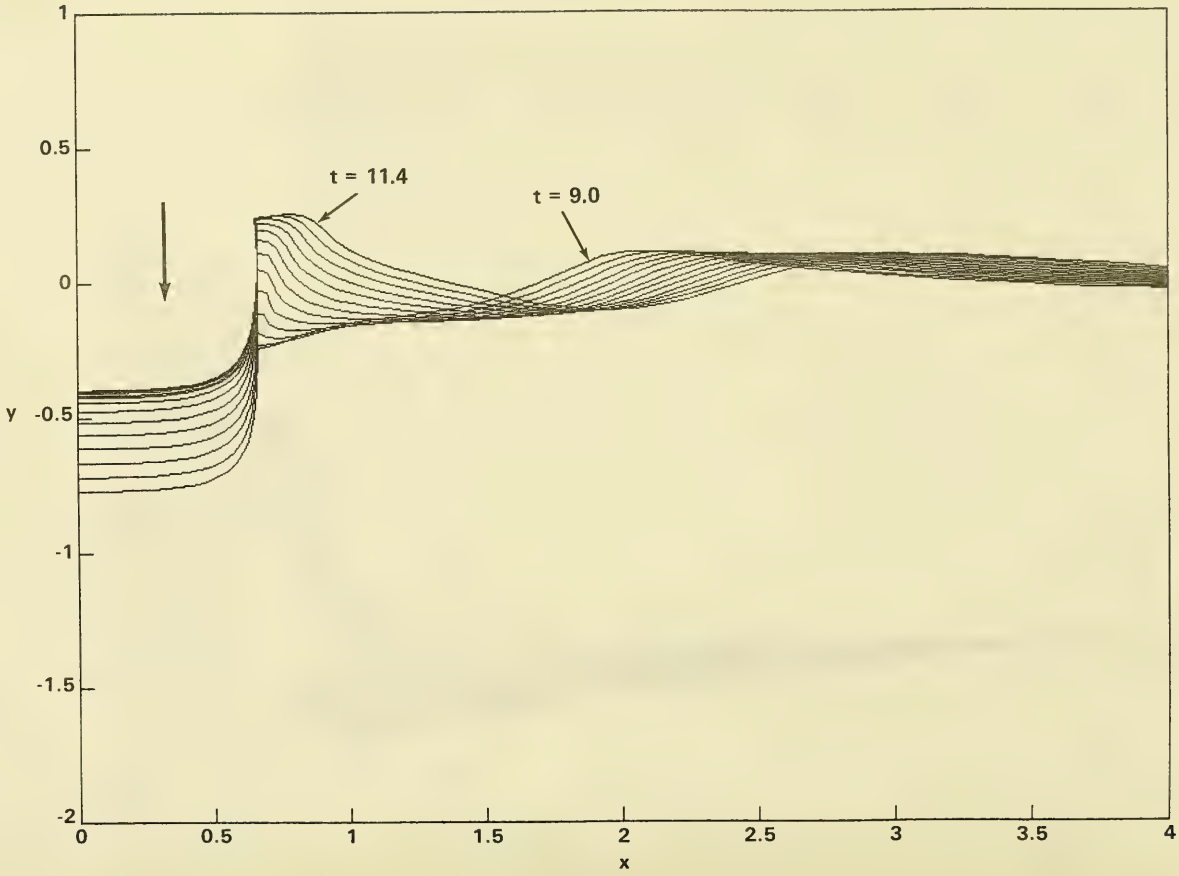

Figure 8 - Free-Surface Elevations Near Body for t = 9.0, 9.2, ..., 11.4

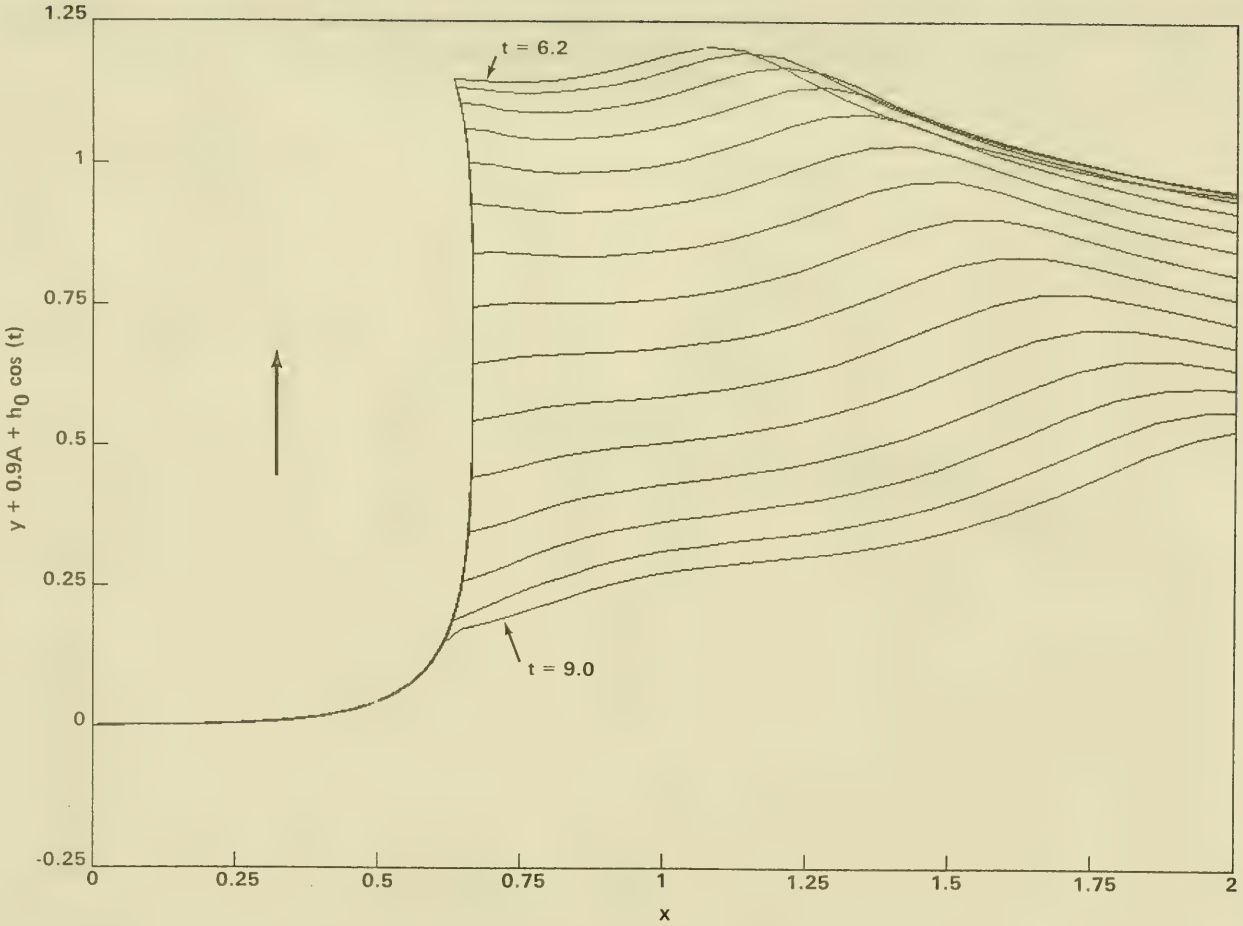

Figure 9 - Free-Surface Positions in a Frame of Reference Fixed to the Body for t = 6.2, 6.4, ..., 9.0

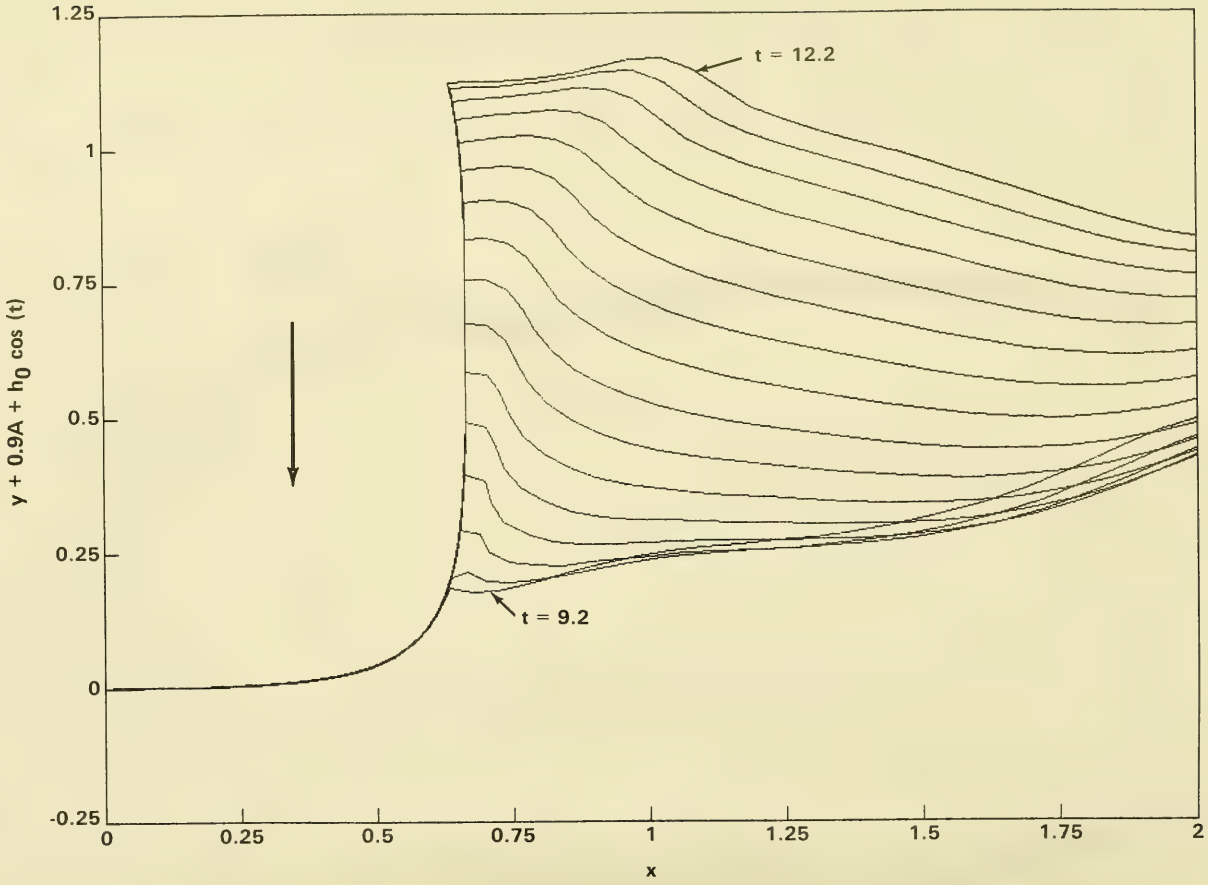

Figure 10 - Free-Surface Positions in a Frame of Reference Fixed to the Body for t = 9.2, 9.4, ..., 12.2

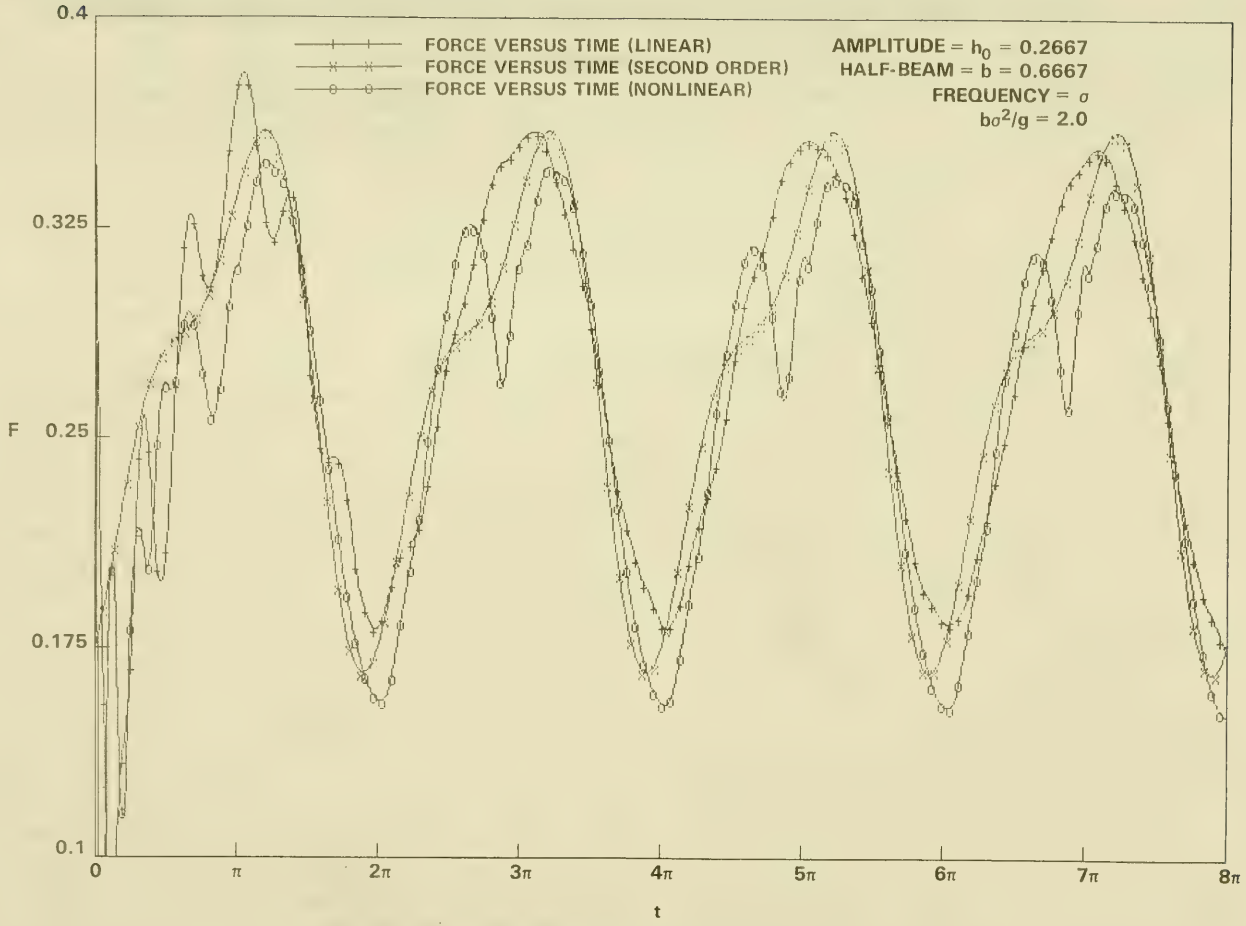

Figure 11 - Comparison of Computed Nonlinear Force with Linear Force and with Second-Order Force as Functions of Time t

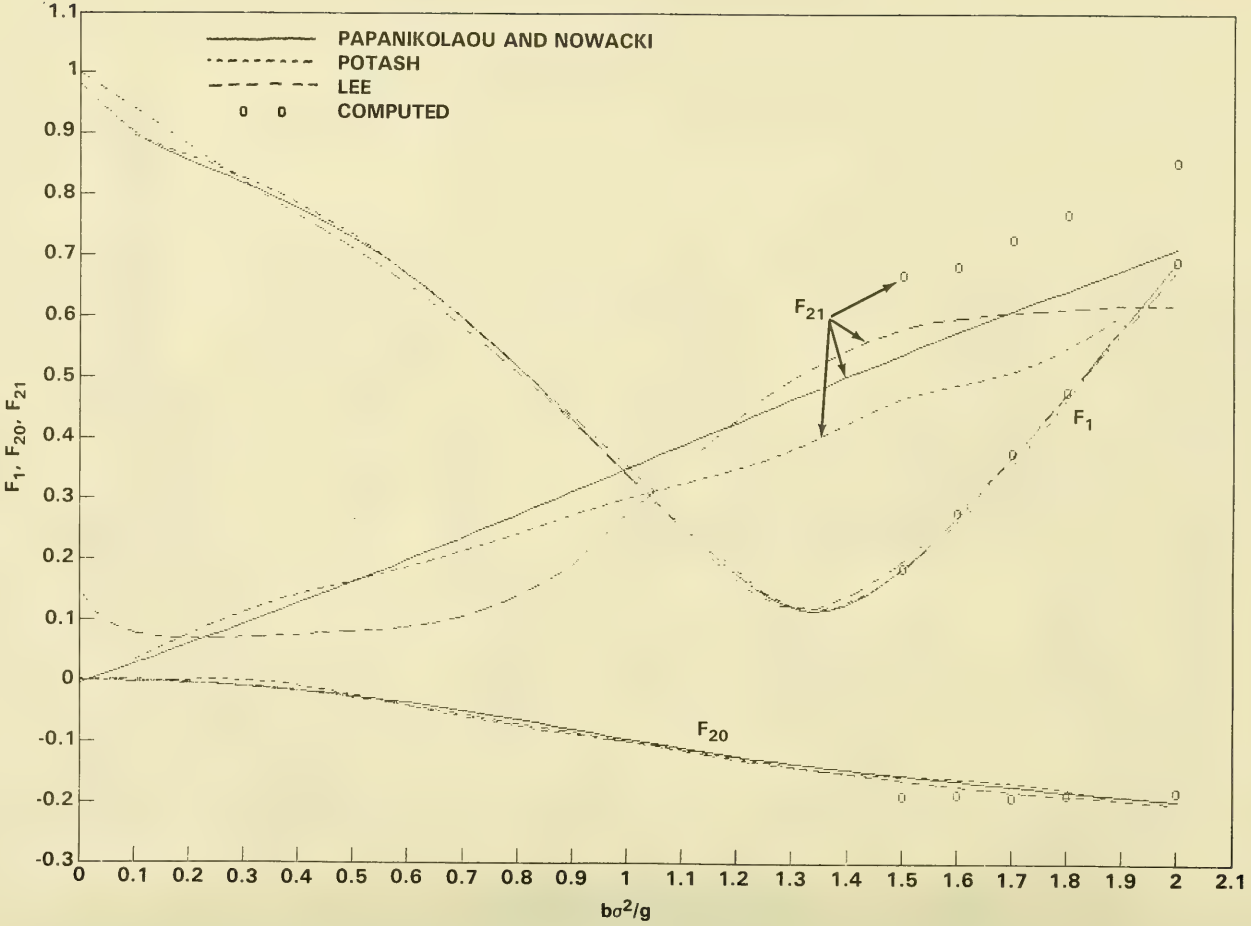

Figure 12 - First- and Second-Order Forces versus Frequency Number for U-Shaped Cylinder

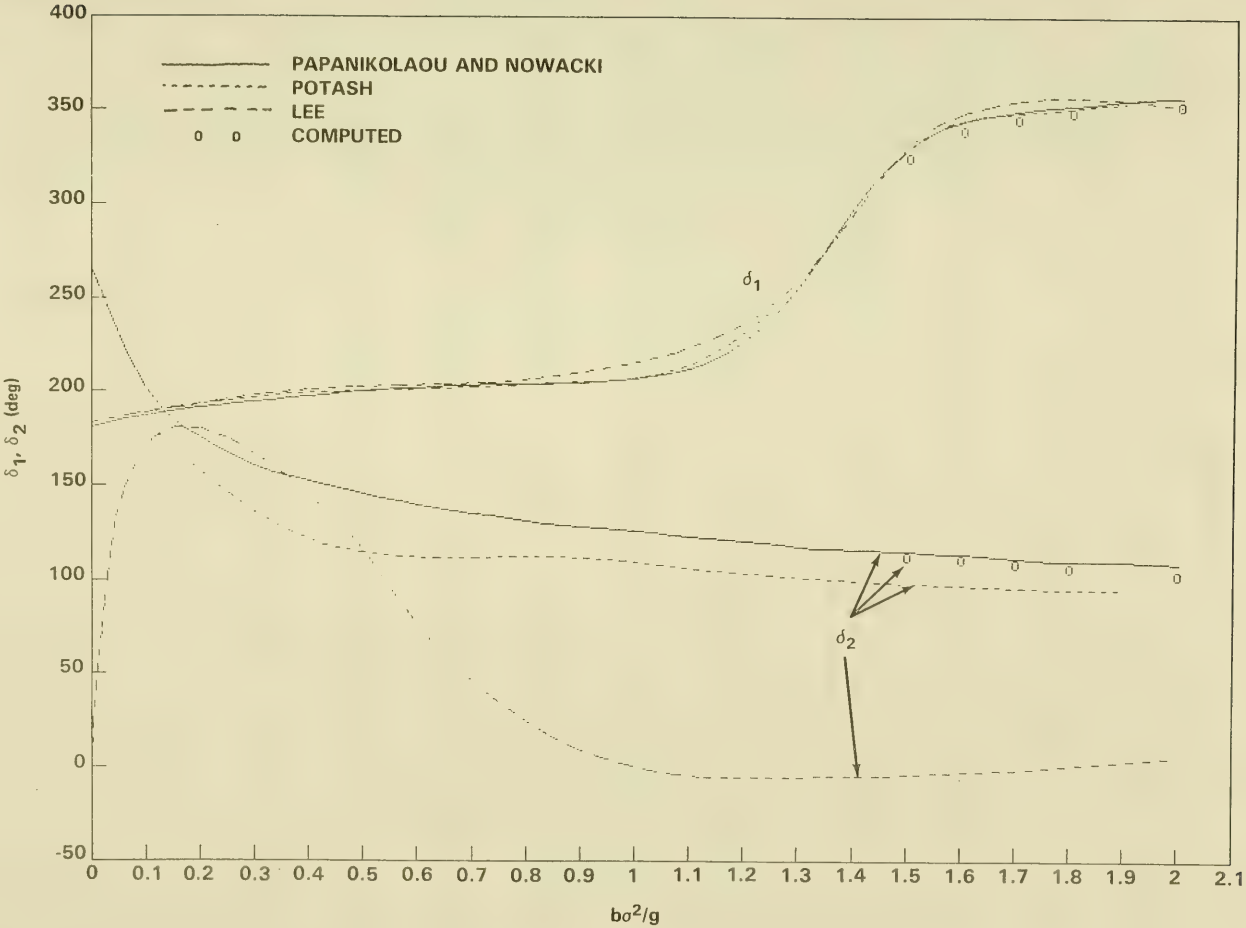

Figure 13 - Phase Angle of Forces of First- and Second-Order versus Frequency Number for U-Shaped Cylinder

REFERENCES

[1] Lin, W.-M., J.N. Newman, and D.K. Yee, "Nonlinear Forced Motions of Floating Bodies," Proceedings of the Fifteenth Symposium on Naval Hydrodynamics, Hamburg (Sep 1984).

[2] Dagan, G., and M.P. Tulin, "Two-Dimensional Free-Surface Gravity Flow Past Blunt Bodies," Journal of Fluid Mechanics, Vol. 51, pp. 529-543 (1972).

[3] Fernandez, G., "Nonlinearity of the Three-Dimensional Flow Past a Flat Blunt Ship," Journal of Fluid Mechanics, Vol. 108, pp. 345-361 (1981).

[4] Longuet-Higgins, M.S., and E.D. Cokelet, "The Deformation of Steep Surface Waves on Water, I: A Numerical Method of Computation," Proceedings of the Royal Society of London, Series A, Vol. 350, pp. 1-26 (1976).

[5] Faltinsen, O.M., "Numerical Solutions of Transient Nonlinear Free-Surface Motion Outside or Inside Moving Bodies," Proceedings of the Second International Conference on Numerical Ship Hydrodynamics, Berkeley, Calif. (Sep 1977).

[6] Vinje, T., and P. Brevig, "Breaking Waves on Finite Water Depths: A Numerical Study," Ship Research Institute of Norway Report R-111.81 (Mar 1981).

[7] Vinje, T., and P. Brevig, "Nonlinear, Two-Dimensional Ship Motions," Ship Research Institute of Norway Report R-112.81 (Mar 1981).

[8] Vinje, T., and P. Brevig, "Nonlinear Ship Motion," Proceedings of the Third International Conference on Numerical Ship Hydrodynamics, Paris (Jun 1981).

[9] Greenhow, M., T. Vinje, P. Brevig, and J. Taylor, "A Theoretical and Experimental Study of the Capsize of Salter's Duck in Extreme Waves," Journal of Fluid Mechanics, Vol. 118, pp. 259-275 (1982).

[10] Baker, G.R., D.I. Meiron, and S.A. Orszag, "Applications of a Generalized Vortex Method to Nonlinear Free Surface Flows," Proceedings of the Third International Conference on Numerical Ship Hydrodynamics, Paris (Jun 1981).

[11] Haussling, H.J., "Solution of Nonlinear Water Wave Problems Using Boundary-Fitted Coordinate Systems," Numerical Grid Generation, edited by Joe F. Thompson, North-Holland (1982).

[12] Shapiro, R., "Linear Filtering," Mathematics of Computation, Vol. 29, pp. 1094-1097 (1975).

[13] Ohring, S., and J. Telste, "Numerical Solutions of Transient Three-Dimensional Ship-Wave Problems," Proceedings of the Second International Conference on Numerical Ship Hydrodynamics, Berkeley, Calif. (Sep 1977).

[14] Haussling, H.J., and R.M. Coleman, "Finite-Difference Computations Using Boundary-Fitted Coordinates for Free-Surface Potential Flows Generated by Submerged Bodies, "Proceedings of the Second International Conference on Numerical Ship Hydrodynamics, Berkeley, Calif. (Sep 1977).

[15] Thompson, J.F., F.C. Thames, and C.W. Mastin, "Automatic Numerical Generation of Body-Fitted Curvilinear Coordinate System for Field Containing Any Number of Arbitrary Two-Dimensional Bodies," Journal of Computational Physics, Vol. 15, pp. 299-319 (1974).

[16] Coleman, R.M., and H.J. Haussling, "Nonlinear Waves Behind an Accelerated Transom Stern," Proceedings of the Third International Conference on Numerical Ship Hydrodynamics, Paris (Jun 1981).

[17] Lee, C.M., "The Second-Order Theory of Heaving Cylinders in a Free Surface," Journal of Ship Research, Vol. 12, pp. 313-327 (1968).

[18] Papanikolaou, A. and H. Nowacki, "Second-Order Theory of Oscillating Cylinders in a Regular Steep Wave," Proceedings of the Thirteenth Symposium on Naval Hydrodynamics, Tokyo (1980).

[19] Potash, R., "Second-Order Theory of Oscillating Cylinders," Journal of Ship Research, Vol. 15, pp. 295-324 (1971).

INITIAL DISTRIBUTION

Copies		
7	CONR	
	1	400 Saalfeld
	1	411 Wegman
	1	411MA Holland
	1	432 Whitehead
	3	432F Lee
4	NRL	
	1	2627
	1	5840 Skop
	1	5841 Griffin
	1	5844 Hansen
5	NAVSEA	
	1	Library
	1	05R24
	1	55W3 Comstock
	2	55W33 Sandberg
		Chen
3	NAVPGSCOL	
	1	Sarpkaya
	1	Math Dept
	1	Library
1	NUSC	
	Tech Lib	
1	NSWC/Dahlgren/Lib	
3	NSWC/Whiteoak	
	1	Library
	2	R44 Solomon
		Zien
1	NAVWARCOL	
1	NAVSHIPYD BREM/Lib	
1	NAVSHIPYD CHASN/Lib	
1	NAVSHIPYD MARE/Lib	
1	NAVSHIPYD NORVA/Lib	

Copies	
1	NAVSHIPYD PEARL/Lib
1	NAVSHIPYD PHILA/Lib
1	NAVSHIPYD PTSMH/Lib
1	Naval Coastal System Cent Tech Lib
1	Naval Ocean Systems Cent Tech Lib
1	Naval Ship Eng Cent Tech Lib
1	Coast Guard Headquarters Librarian Station 5-2 NASSIF Building
1	Library of Congress Science and Tech Division
1	Scientific Advisor Commandant of the Marine Corps Dr. A.L. Slafkosky Code AX
2	Maritime Administration 1 Office of Maritime Tech 1 Div of Naval Arch
2	USNA 1 Tech Lib 1 B. Johnson
12	DTIC
1	BUSTAND/Lib
1	NASA HQS/Lib
1	NASA Scientific and Tech Information Facility

Copies

5 NASA Ames Res Cen
- 1 Kwak
- 1 Martin
- 1 MacCormick
- 1 Sorenson
- 1 Lib

1 NASA Lewis Res Cen/Lib

1 NASA Marshall SFC/Lib

1 NASA Langley Res Cen
- 1 D. Bushnell

1 Brown University
Division of Engineering
J.T.C. Liu

5 California Institute of Tech
- 1 A. Roshko/Grad Aero Lab
- 1 P.G. Saffman/Dept of Applied Math
- 2 C.E. Brennen/ A.J. Acosta/Dept of Mech Eng
- 1 T.Y. Wu/Dept of Eng Sci

1 Calif State Univ/Long Beach
Mech Eng Dept
T. Cebeci

1 Case Western Reserve Univ
Dept of Mech & Aero Eng
E. Reshotko

1 Colorado State University
Dept of Mathematics
J.W. Thomas

2 Cornell University
Sibley School of Mech & Aerospace Eng
- 1 J.L. Lumley
- 1 S.F. Shen

Copies

4 Johns Hopkins University
- 1 S. Corrsin/Dept of Chem Eng
- 1 O.M. Phillips/Dept of Earth & Planetary Sci
- 1 T.D. Taylor/Applied Physics Laboratory
- 1 R.E. Gibson Library/ Applied Physics Lab

1 Lehigh University
Dept of Mech Eng and Mech
D. Rockwell

5 MIT
- 1 C.C. Mei/Dept of Civil Eng
- 4 Dept of Ocean Eng
  - 1 Library
  - 1 P. Leehey
  - 1 J.E. Kerwin
  - 1 J.N. Newman

1 Michigan State University
Dept of Mech Eng
R.E. Falco

1 Mississippi State University
Dept of Aerospace Eng
Drawer A
J.F. Thompson

1 Pennsylvania State Univ
Library/Applied Research Lab
PO Box 30

1 Princeton University
Dept. of Chemical Eng
W.R. Schowalter

1 Purdue University
School of Mech Eng
W.G. Tiederman

3 Stevens Institute of Technology
Davidson Laboratory
- 2 D. Savitsky
- 1 Library

Copies	
7	Univ of Calif/Berkeley 2 Dept of Mech Eng 1 S.A. Berger 1 P.M. Naghdi 5 Dept of Naval Arch & Offshore Eng 1 Librarian 3 R.W. Yeung 1 J.W. Wehausen
1	Univ of Calif/La Jolla J.W. Miles
1	University of California Los Alamos Scientific Lab C.W. Hirt
1	Univ of California/San Diego Library/Marine Physical Lab Scripps Institute of Oceanography
1	Univ of Calif/Santa Barbara Dept of Mechanical and Environmental Engineering M.P. Tulin
2	University of Cincinnati Dept of Aerospace Engineering & Applied Mechanics 1 U. Ghia 1 S.G. Rubin
1	University of Delaware College of Marine Studies Jin Wu
1	University of Houston Dept of Mech Eng A.K.M. Fazle Hussain
3	University of Iowa Inst of Hydraulic Research 1 Library 2 V.C. Patel

Copies	
1	University of Michigan Dept of Aerospace Eng W.W. Willmarth
4	University of Michigan 1 Library 1 R.F. Beck 1 W.S. Vorus 1 F.T. Ogilvie
1	University of Minnesota Lorenz G. Straub Library St. Anthony Falls Hydraulic Lab
2	University of Southern Calif Dept of Aerospace Eng C.M. Ho
1	University of Southern Calif Dept. of Mech Eng T. Maxworthy
1	Univ of Texas/Austin Library/Applied Research Lab
2	Stanford University 1 R.L. Street 1 J.B. Keller
1	University of Tennessee Dept of Engineering, Science and Mechanics A.J. Baker
3	Virginia Polytechnic Inst and State University 1 A.H. Nayfeh 2 J. Schetz
1	Webb Inst of Naval Arch Technical Library
1	Woods Hole Oceanographic Inst Library
1	Soc of Naval Architects and Marine Engineers

Copies	
1	Applied Mechanics Review Southwest Research Inst
1	Engineering Societies Lib
1	Southwest Research Institute Library
1	Cambridge Hydrodynamics, Inc S.A. Orszag
1	Ecodynamics Research Associates P.J. Roache
1	Flow Research Company J.H. Duncan
1	Nielsen Eng & Research G.D. Kerlick
1	Science Applications, Inc. N. Salvesen
1	Scientific Research Associates, Inc. S.J. Shamroth

CENTER DISTRIBUTION

Copies	Code	Name
1	01	A. Powell
1	012	E. O'Neill
1	012.3	D. Moran
1	012.4	R. Stevens
1	12	W. Dietz
1	15	W.B. Morgan
1	1504	V.J. Monacella
1	152	W.C. Lin
1	154	J.H. McCarthy
1	154.1	B. Yim
2	1542	T. Huang F. Noblesse
1	1543	E.P. Rood
1	1544	A. Reed
1	156	D.S. Cieslowski
1	16	H. Chaplin
2	1606	T.C. Tai H. Berman
1	17	
1	18	G.H. Gleissner
1	1802	H. Lugt
2	1809.3	
1	182	A.W. Camara
1	184	J.W. Schot
1	1843	H.J. Haussling
30	1843	J.G. Telste
1	1844	S.K. Dhir
1	185	T. Corin
1	189	G. Gray
1	19	M.M. Sevik
1	1905.1	W.K. Blake
1	2704	E. Quandt
1	2721	R.K. Muench

Copies	Code	Name
1	2722	B.B. Hwang
1	272T	H. Urbach
1	274	L. Agiro
1	283	H. Singerman
1	2862	P.D. Conroy
10	5211.1	Reports Distribution
1	522.1	TIC (C)
1	522.2	TIC (A)

DTNSRDC ISSUES THREE TYPES OF REPORTS

1. DTNSRDC REPORTS, A FORMAL SERIES, CONTAIN INFORMATION OF PERMANENT TECHNICAL VALUE. THEY CARRY A CONSECUTIVE NUMERICAL IDENTIFICATION REGARDLESS OF THEIR CLASSIFICATION OR THE ORIGINATING DEPARTMENT.

2. DEPARTMENTAL REPORTS, A SEMIFORMAL SERIES, CONTAIN INFORMATION OF A PRELIMINARY, TEMPORARY, OR PROPRIETARY NATURE OR OF LIMITED INTEREST OR SIGNIFICANCE. THEY CARRY A DEPARTMENTAL ALPHANUMERICAL IDENTIFICATION.

3. TECHNICAL MEMORANDA, AN INFORMAL SERIES, CONTAIN TECHNICAL DOCUMENTATION OF LIMITED USE AND INTEREST. THEY ARE PRIMARILY WORKING PAPERS INTENDED FOR INTERNAL USE. THEY CARRY AN IDENTIFYING NUMBER WHICH INDICATES THEIR TYPE AND THE NUMERICAL CODE OF THE ORIGINATING DEPARTMENT. ANY DISTRIBUTION OUTSIDE DTNSRDC MUST BE APPROVED BY THE HEAD OF THE ORIGINATING DEPARTMENT ON A CASE-BY-CASE BASIS.